SEISMIC ANALYSES OF AN EARTH DAM USING THE BOUNDING SURFACE PLASTICITY MODEL

Dr. Omar al-Farouk Salem Al-Damluji
Assistant Professor
Department of Civil Engineering,
University of Baghdad, Iraq.

ABSTRACT

This investigation presents coupled analyses of an earth-dam problem including all aspects of fluid-structure interaction (class I coupling) and soil-pore fluid–structure interaction (class II coupling) under earthquake excitations using the finite element method and its comparison with the uncoupled one. New software for predicting and analyzing coupled behaviour is established using the pressure formulation for modelling of the fluid and the u-p formulation for modelling of the soil-pore fluid. The staggered partitioned solution technique for coupled field problems is implemented and used in the computer code. This scheme is incorporated in terms of a sequential execution for single-field analyzers. The bounding surface plasticity model is used as a constitutive relationship for modelling the clay core of a dam made up of Boston blue clay first and Baghdad brown silty clay later. The general theoretical framework of the model and its numerical implementation with emphasis on isotropic cohesive soils are given. Also, the input material parameters are identified and the tests required for determining these parameters are clarified on Baghdad brown silty clay. Implicit-Implicit Newmark's numerical integration scheme with a corrector / predictor algorithm is employed for time integration of the equations of motion.

The results show that the bounding surface plasticity model can give a logical impression for the behaviour of clayey soils under dynamic loads. Also, the earthquake design of structures generally and dams, in particular, must take into account various interactions between the foundation, the structure and the water in the reservoir in addition to site effects. Amplifications due to stratification and dephasing (response lag) in the foundations of structures should also be considered.

الخلاصة

يتطرق هذا البحث الى اجراء تحليل مزدوج لمسألة سد ترابي متضمنا كافة جوانب التفاعل المتبادل بين المائع و المنشأ (ازدواج من الصنف الأول) فضلا عن تفاعل متبادل بين التربة و مائع المسام و المنشأ (ازدواج من الصنف الثاني) تحت هزة ارضية باستخدام طريقة العناصر المحددة. لقد تم استخدام برامجيات مطورة تتوقع و تحلل التصرف المزدوج بالاعتماد على معادلة الضغط لنمذجة المائع و معادلة الازاحة – الضغط لنمذجة مائع مسام التربة. لقد تم استخدام طريقة حل التقسيم المتعرج لمسائل المجال المزدوج. كما تم استخدام نموذج لدونة السطح المحيطي كعلاقة تكوينية تمثل تصرف اللب الطيني للسد باستخدام تربة طين بوسطن الأزرق و تربة طين غرين بغداد البني. لقد تم ادراج الهيكل النظري العام للنموذج مع التأكيد على الترب المتماسكة المتماثلة. كما تم تحديد الفحوص الحقلية و المختبرية لتربة طين غرين بغداد البني و ادراج

النتائج المستحصلة عنها و لقد تم استخدام طريقة تكامل نيومارك العددية الضمنية مع خوارزمية التصـــليح \ التوقع لاجراء عمليات التكامل الزمني لمعادلات الحركة.

تبين النتائج امكانية اعطاء نموذج لدونة السطح المحيطي نظرة منطقية لتوقع تصرف الترب الطينية تحت احمال حركية. كمـــا يجب ان تأخذ تصاميم الهزات الأرضية بنظر الأعتبار التفاعلات المتبادلة بين الأساس و المنشأ الترابي و ماء خـــزان الســـد اضافة الى التأثيرات الموقعية.

KEY WORDS
coupled analysis, earth dam-reservoir, finite element method, fluid-structure interaction, soil-pore-fluid interaction, pressure formulation, u-p formulation, bounding surface plasticity model, Baghdad brown silty clay, Boston blue clay.

INTRODUCTION

Soil plasticity problems are nonlinear and time-dependent and thus require more elaborate solution schemes for such boundary value problems than simple linear elasticity cases. In general, all techniques for nonlinear analysis can, with certain qualifications, be applied irrespective of the constitutive law, although some of them are better suited to particular laws than others (Naylor and Pande, 1981).

Several studies have considered the use of the bounding surface plasticity model as one of the universal history-dependent constitutive models for clayey soils (Al-Damluji (1994) and his coworkers at the University of Baghdad (Abbas (2003), Al-Ani (2001), Al-Busoda (2004), Al-Ebady (2001), Al-Juboory (2003), Al-Nu'aimi (2004), Al-Sherefi (2000) and Al-Tae'e (2001)), Dafalias (1975, 1980, 1986), Dafalias and Herrmann (1980, 1982, 1986), Herrmann et al. (1987), Mroz and Zienkiewicz (1984) and Mroz et al. (1978, 1979).

FLUID-STRUCTURE AND SOIL-PORE FLUID INTERACTIONS

The dynamic analysis of soil-fluid-structure interaction, as depicted in earth dam analyses, includes all aspects of both fluid and solid mechanics (i.e., fluid-structure interaction (class I coupling) and soil-pore-fluid interaction (class II coupling)). In a fluid phase, the viscosity of the fluid, the magnitude of the gradient of the velocity field throughout the flow and whether the fluid is compressible or incompressible, depending on whether density variations are large or small, play a key role in choosing the kind of formulation used. However, in the solid phase, the time scale and the solver algorithm to be used depends on the loading rate and the permeability of the porous medium (Al-Damluji et al, 2005). In this study, a non-flow problem is considered where the water in the reservoir is impounded. Flow occurs only due to the application of the externally applied load being an earthquake load under consideration herein.

Class I Coupling - Fluid-Structure Interaction

From mass conservation, the continuity equation for a flowing fluid is derived as (Frank):

$$\dot{\rho}_f + (\rho_f \underline{\dot{u}}_f)_{,i} = 0 \equiv \dot{\rho}_f + \underline{\nabla}\,(\rho_f \underline{\dot{u}}) \qquad (1)$$

or $$\partial \rho_f / \partial t + \partial(\rho_f \dot{u}_x)/\partial x + \partial(\rho_f \dot{u}_y)/\partial y + \partial(\rho_f \dot{u}_z)/\partial z = 0$$

where: ρ_f = the mass density, $\underline{\dot{u}} = \hat{i}\,\dot{u}_x + \hat{j}\,\dot{u}_y + \hat{k}\,\dot{u}_z$, $\hat{i}$, $\hat{j}$, $\hat{k}$ are unit vectors in x, y and z directions, respectively, $\underline{\nabla} = \hat{i}(\partial/\partial x) + \hat{j}(\partial/\partial y) + \hat{k}(\partial/\partial z)$, t = the time, and $\dot{u}_x$, $\dot{u}_y$ and $\dot{u}_z$ = the velocity components (for the fluid) in x, y and z directions, respectively.

From momentum conservation of the inviscid fluid and for incompressible flow :

$\rho_f \ddot{v}_i = -P_{,i} + \mu' \ddot{v}_{i,kk}$. (2)

Pressure Formulation

The linearized Navier-Stokes equation is given by (Joseph):

$\nabla^2 P + \xi' \nabla^2 \dot{P} = \ddot{P}/c^2$ (Linearized-Navier-Stokes Equation) (3)

where: $\xi' = 4\mu'/3\ \rho_f c^2$, μ' = the dynamic viscosity of fluid and $c = (K/\rho)^{1/2}$ (the velocity of the waves through the fluid) .

For an inviscid fluid, the above equation reduces to :

$\nabla^2 P = \ddot{P}/c^2$.(4)

The equation of motion can be expressed, after spatial discretization, by two sets of second order differential equations. However, in this study, the pressure formulation is used in which the coupled fluid-structure equation can be expressed as:

$\underline{M}_s \ddot{\underline{u}} + \underline{C}_s \dot{\underline{u}} + \underline{K}_s \underline{u} = \underline{f}_s - \underline{M}_s \ddot{\underline{d}} + \underline{L}\, \underline{P}$ (5)

$\underline{M}_f \ddot{\underline{P}} + \underline{C}_f \dot{\underline{P}} + \underline{K}_f \underline{P} = \underline{f}_f - \rho_f \underline{L}^T (\ddot{\underline{u}} + \ddot{\underline{d}})$ (6)

where:

$\underline{M}_s = \int_\Omega \underline{N}_u^T \rho \underline{N}_u d\Omega$ (7a)

$\underline{C}_s = \alpha \underline{M}_s + \beta \underline{K}_s$ (Rayleigh Damping) (7b)

$\underline{K}_s = \int_\Omega \underline{B}^T \underline{D}_T \underline{B} d\Omega$ (7c)

$\underline{f}_s = \int_{\Gamma u} \underline{N}_u^T \underline{t}\, d\Gamma + \int_\Omega \underline{N}_u^T \rho\, \underline{b}\, d\Omega + \int_\Omega \underline{B}^T \underline{D}^T d\underline{\varepsilon}^0\, d\Omega$.(7d)

$\underline{L} = \int_\Omega \alpha_c \underline{B}^T \underline{\delta}\, \underline{N}_p\, d\Omega$ (7e)

$(\underline{M}_f)_{ij} = \int_{\Gamma F} \underline{N}_{pi}\, 1/g\ \underline{N}_{pj}\, d\Gamma + \int_{\Omega F} \underline{N}_{pi}^T\, 1/c^2\ \underline{N}_{pj}\, d\Omega$ (7f)

$(\underline{C}_f)_{ij} = \int_{\Gamma R} \underline{N}_{pi}^T\, 1/c^2\ \underline{N}_{pj}\, d\Gamma$ (7g)

$(\underline{K}_f)_{ij} = \int_{\Omega F} (\nabla \underline{N}_{pi})^T\, (\nabla \underline{N}_{pj})\, d\Omega$.(7h)

$(\underline{L}^T)_{ij} = \int_{\Gamma I} \underline{N}_{ui}^T\, n\, \underline{N}_{pj}\, d\Gamma$ (7i)

Special Cases for Class I Coupling

Rigid structure and incompressible fluid

The assumption of a rigid structure implies that Equation (5) vanishes and that Equation (6) reduces to:

$\underline{K}_f \underline{P} = -\rho_f \underline{L}^T \ddot{\underline{d}}$.(8)

Rigid structure and compressible fluid

Again consideration of a rigid structure implies that Equation (5) vanishes and Equation (6) reduces to:

$\underline{M}_f \ddot{\underline{P}} + \underline{C}_f \dot{\underline{P}} + \underline{K}_f \underline{P} = -\rho_f \underline{L}^T \ddot{\underline{d}}$ (9)

Flexible Structure and Incompressible Fluid

For an incompressible fluid, the speed of sound c in the fluid is taken to be infinity. The matrices $\underline{M}_f$ and $\underline{C}_f$ in Equation (6), therefore, vanish and the equations reduce to:

$$\underline{M}_s \ddot{\underline{u}} + \underline{C}_s \dot{\underline{u}} + \underline{K}_s \underline{u} = \underline{f}_s - \underline{M}_s \ddot{\underline{u}}_g + \underline{L}\,\underline{P} \quad (10)$$

$$\underline{K}_f \underline{P} = -\rho_f \underline{L}^T (\ddot{\underline{u}} + \ddot{\underline{u}}_g) \quad (11)$$

Solving Equation (11) for $\underline{P}$, gives:

$$\underline{P} = -\rho_f \underline{K}_{f_e}^{-1} \underline{L}^T (\ddot{\underline{u}} + \ddot{\underline{u}}_g) \quad (12)$$

and substituting equation (12) in Equation (10) gives:

$$\underline{M}_{sf} \ddot{\underline{u}} + \underline{C}_s \dot{\underline{u}} + \underline{K}_s \underline{u} = \underline{f}_s - \underline{M}_{sf} \ddot{\underline{u}}_g \quad (13)$$

where: $\underline{M}_{sf} = \underline{M}_s + \underline{M}_{ff}$ and $\underline{M}_{ff} = \rho_f \underline{L}\, \underline{K}_f^{-1} \underline{L}^T$ (added mass).

Class II Coupling - Pore–Fluid–Solid Interaction (u-p Formulation)

When the seepage velocity relative to the solid skeleton is small compared with the motion of the solid skeleton or if the permeability is low, the relative acceleration of the fluid with respect to the solid can be neglected. With this approximation (i.e., neglecting $\ddot{w}$ term) and replacing the unknown w with the pressure P, the equilibrium equation of the fluid can be rewritten as (Paul, 1982):

$$\dot{w} = -k \nabla P + k\rho \underline{b} - k\rho \ddot{\underline{u}} \quad (14)$$

which can be used to eliminate w from the continuity equation. Upon discretization, it is possible to write:

$$\underline{u} = \underline{N}_u \underline{u} \quad (15)$$

$$\underline{P} = \underline{N}_p P \quad (16)$$

and using the standard Galerkin method, the resulting equations can be expressed as:

$$\underline{M}_s \ddot{\underline{u}} + \underline{C}_s \dot{\underline{u}} + \underline{K}_s \underline{u} = \underline{f}_s - \underline{M}_s \ddot{\underline{u}}_g + \underline{L}\,\underline{P} \quad (17)$$

$$\underline{C}_P \dot{\underline{P}} + \underline{K}_P \underline{P} = \underline{f}_P - \underline{L}^T \dot{\underline{u}} + \hat{\underline{M}} \ddot{\underline{u}}_g \quad (18)$$

where:

$$\underline{K}_s = \int_\Omega \underline{B}^T (\underline{D}_T + \alpha_c^2 \delta.Q.\delta^T) \underline{B}\, d\Omega \quad (19a)$$

$$\underline{C}_p = \int_\Omega \underline{N}_p^T\, 1/Q\, \underline{N}_p\, d\Omega \quad (19b)$$

$$\underline{K}_p = \int_\Omega (\nabla \underline{N}_p)^T\, k\, (\nabla \underline{N}_p)\, d\Omega \quad (19c)$$

$$\underline{f}_p = \int_{\Gamma_p} \underline{N}_p^T\, P\, d\Gamma + \int_\Omega (\nabla \underline{N}_p)^T\, k\, \rho_f\, \underline{b}\, d\Omega \quad (19d)$$

$$\underline{L}^T = \int_\Omega \alpha_c\, \underline{N}_p^T\, \delta\, \underline{B}\, d\Omega \quad (19e)$$

$$\hat{\underline{M}} = \int_\Omega (\nabla \underline{N}_p)^T\, k\, \rho_f\, \underline{N}_u\, d\Omega \quad (19f)$$

and where: $\underline{N}_p$ and $\underline{N}_u$ are the shape functions used for pore pressure and solid skeleton, respectively. α and β are Rayleigh damping constants, Ω = the domain, Γ = the boundary surface, $\underline{B}$ = the strain displacement matrix and t = the surface traction. In this study, this formulation is implemented and used in the computer program for coupled analysis. Uncoupled analysis would imply the use of Equation (17) only without the last term on the right hand side of it.

A STAGGERED SOLUTION SCHEME

Problems involving more than one field variable, such as soil-structure interactions, are often partitioned into well defined fields which are distinct in behavior, material model or solution technique. The staggered partitioned solution scheme for the coupled field problem is implemented and used in the computer code used in the analysis herein.

A computer code was developed, implemented and verified depending on Equations (17-19) and using the staggered time marching scheme (Al-Damluji et al, 2005 and Al-Nu'aimi, 2004). It is used for analyzing the problem under consideration in the study herein.

A BOUNDING SURFACE PLASTICITY MODEL FOR CLAYS

The adoption of refined constitutive models for the clay core is of essence for obtaining realistic solutions of the behaviour of zoned earth dams under earthquake excitations. The bounding surface plasticity model is best suited for such problems (Al-Damluji and Al-Ta'ee, 2002 and Al-Juboory, 2003). A two-surface model of this type is proposed by Mroz et al. (1978, 1979) for clays and implemented by Kaliakin and others (1990 and 1987).

General Aspects of the Bounding Surface Concept

It is well known that the total strain rate $\dot{\varepsilon}_{ij}$ can be divided into elastic and plastic parts as (Desai and Siriwardane, 1984):

$$\dot{\varepsilon}_{ij} = \dot{\varepsilon}^{e}_{ij} + \dot{\varepsilon}^{p}_{ij} \qquad (20)$$

where: a superposed dot indicates the rate, ε_{ij} = strains due to stresses and the superscripts e and p denote the elastic and plastic parts.

The constitutive law relating the elastic rates is given by:

$$\dot{\varepsilon}^{e}_{ij} = C_{ijkl}\,\dot{\sigma}_{kl} \;;\quad \dot{\sigma}_{ij} = E_{ijkl}\,\dot{\varepsilon}^{e}_{kl} \qquad (21)$$

where: C_{ijkl} describes the components of the elasticity tensor, and E_{ijkl} is the inverse of C_{ijkl}, both are fourth order tensors. The components of these moduli are assumed to be functions of the stress σ_{ij} and directional properties.

Now, if L_{ij} = the loading direction, R_{ij} = the direction of $\dot{\varepsilon}^{p}_{ij}$ and r_n = the "direction " of $\dot{\varepsilon}_n$, then the plastic rate equations of evolution and the total strain rate-stress rate relations for an elastoplastic state can be expressed by (Dafalias, 1986):

$$\dot{\varepsilon}^{p}_{ij} = \langle L \rangle\, R_{ij} \qquad (22)$$

$$\dot{\varepsilon}_{n} = \langle L \rangle\, r_{n} \qquad (23)$$

$$\dot{\sigma}_{ij} = D^{-1}_{ijkl}.\dot{\varepsilon}_{kl} \qquad (24)$$

$$D_{ijkl} = E_{ijkl} - \bar{h}.(L).B^{-1}.P_{ij}.Q_{kl} \qquad (25)$$

$$Q_{kl} = E_{klrs}.L_{rs}\,,\quad P_{ij} = E_{ijab}.R_{ab} \qquad (26)$$

$$B = K_p + L_{ab}.E_{abcd}.R_{cd} \qquad (27)$$

$$L = \frac{1}{K_p} L_{ij}.\dot{\varepsilon}_{ij} = \frac{1}{B} Q_{kl}.\dot{\sigma}_{kl} \qquad (28)$$

where: K_p = the plastic modulus, L = the loading index, $\bar{h}(L)$ = the Heaviside step function defined as 1 for $L > 0$ and 0 at $L \le 0$ and the Macauley brackets $\langle\ \rangle$ defining the operation $\langle L \rangle = \bar{h}(L)L$.

The Radial Mapping Rule

Radial mapping is one of the particular formulations of the bounding surface plasticity models. This rule is defined as: for any certain direction on the boundary surface, the mapping rule associates the

actual stress point within (or on) the bounding surface, to a corresponding 'image' stress point on the surface, as the intersection of the surface with the straight (radial) line connecting the origin (always within the bounding surface) with the current stress point.

The bounding surface can be described analytically as (Dafalias, 1986):

$$F(\bar{\sigma}_{ij} - \beta_{ij}, q_n) = 0 \qquad (29)$$

The concept of radial mapping, as proposed by Dafalias (1986) will take the form:

$$\bar{\sigma}_{ij} = b(\sigma_{ij} - \alpha_{ij}) + \alpha_{ij} \qquad (30)$$

where b is ≥ 1 and can be determined by inserting the $\bar{\sigma}_{ij}$ from Equation (30) into the analytical expression of $F = 0$. When $\sigma_{ij} = \bar{\sigma}_{ij}$, b is equal to 1, i.e., the identity condition is satisfied and $f = 0$ is identical to $F = 0$, while when $\sigma_{ij} = \alpha_{ij}$, b is equal to ∞ and $\bar{\sigma}_{ij}$ is indeterminate. Equation (30) together with the assumption $L_{ij} = \bar{L}_{ij} = \dfrac{\partial F}{\partial \bar{\sigma}_{ij}}$ define indirectly a loading surface $f = 0$. The following form will be adopted (Dafalias and Herrmann, 1982):

$$K_p = \bar{K}_p + \hat{H}\frac{\delta}{\langle r - s\delta \rangle} = \bar{K}_p + \hat{H}\left\langle \frac{b}{b-1} - s \right\rangle \qquad (31)$$

in which r = the distance of α_{ij} from σ_{ij}, $\hat{H}$ = a positive shape hardening scalar function of σ_{ij} and q_n, and s is the elastic factor that determines indirectly the "elastic nucleus" which represents the innermost of all loading surfaces.

Bounding Surface Formulation for Isotropic Materials

Elastic isotropy is defined in terms of the tangent moduli C_{ijkl} and their inverse E_{ijkl} by Dafalias and Herrmann (1982) as:

$$E_{ijkl} = K\delta_{ij}\delta_{kl} + G\left(\delta_{ik}\delta_{jl} + \delta_{il}\delta_{jk} - \frac{2}{3}\delta_{ij}\delta_{kl}\right) \qquad (32)$$

in which K and G are the tangent bulk and shear moduli, respectively.

Plastic isotropy implies that all q_n are scalar valued, hence, all state functions depend on the isotropic invariants of σ_{ij}. Since all q_n are scalar valued, the projection center α_{ij} must be an isotropic tensor with a principal value I_c on the I-axis in the stress invariant space, i.e., $\alpha_{ij} = (1/3)I_c\delta_{ij}$. If I_c is as an isotropic back-stress, hence, the radial mapping rule (Equation (30)) will become:

$$\bar{I} = b(I - I_c) + I_c \qquad (33)$$

$$\bar{s}_{ij} = bs_{ij} \Rightarrow \bar{J} = bJ,\ \bar{S} = bS,\ \bar{\alpha} = \alpha \qquad (34)$$

Now, if I_c is equal to I, then Equation (33) will lead to $\bar{I} = I$; this assumption is employed for the bounding surface applied onto a concrete model (Yang et al, 1985) where the surface has no intersection with the positive I-axis. But if the bounding surface intersects the positive I-axis at I_0, one can assume $I_c = CI_0$ with $0 \leq C \leq 1$ where C is a constant or variable. Hence, Equation (33) becomes:

$$\bar{I} = b(I - CI_0) + CI_0 \qquad (35)$$

Substitution of Equation (34) with values of $\bar{s}_{ij}$, $\bar{J}$, and $\bar{S}$ into stress invariant equations for s_{ij}, J and S, respectively, give $\partial\bar{I}/\partial\bar{\sigma}_{ij} = \delta_{ij}$ and the derivatives of $\bar{J}$ and $\bar{\alpha}$ with respect to $\bar{\sigma}_{ij}$. Recalling that $\bar{L}_{ij} = L_{ij} = \partial F/\partial\bar{\sigma}_{ij}$ for the radial mapping model, the equations become:

$$F(\bar{I}, \bar{J}, \alpha, k) = 0 \tag{36}$$

$$L_{ij} = F_{,\bar{I}}\,\delta_{ij} + \frac{F_{,\bar{J}}}{2J}s_{ij} + \frac{\sqrt{3}}{2\cos 3\alpha}\frac{F_{,\alpha}}{bJ}\left[\frac{s_{ik}s_{kj}}{J^2} - 3\left(\frac{S}{J}\right)^3\frac{s_{ij}}{2J} - \frac{2}{3}\delta_{ij}\right] \tag{37}$$

in which a comma followed by the symbol of a quantity as a subscript implies the partial derivative in reference to this quantity and k denotes the set of scalar valued q_n. It will be convenient to introduce a plastic potential U such that $R_{ij} = \partial U/\partial\bar{\sigma}_{ij}$ is obtained by Equation (37). Based on Equation (32), Equations (26-28) become:

$$Q_{ij} = 3KF_{,\bar{I}}\,\delta_{ij} + \frac{GF_{,\bar{J}}}{J}s_{ij} + \frac{\sqrt{3}}{\cos 3\alpha}\frac{F_{,\alpha}}{bJ}\left[\frac{s_{ik}s_{kj}}{J^2} - 3\left(\frac{S}{J}\right)^3\frac{s_{ij}}{2J} - \frac{2}{3}\delta_{ij}\right] \tag{38}$$

$$B = K_p + 9K.F_{,\bar{I}}\,U_{,\bar{I}} + G\left[F_{,\bar{J}}\,U_{,\bar{J}} + \frac{F_{,\alpha}.U_{,\alpha}}{(bJ)^2}\right] \tag{39}$$

$$L = \frac{1}{K_p}\left(F_{,\bar{I}}.\dot{\bar{I}} + F_{,\bar{J}}.\dot{\bar{J}} + \frac{1}{b}F_{,\alpha}.\dot{\alpha}\right) = \frac{1}{K_p}\left(F_{,\bar{I}}.\dot{\bar{I}} + F_{,\bar{J}}.\dot{\bar{J}} + F_{,\alpha}.\dot{\alpha}\right) = \frac{Q_{kl}\dot{\bar{\sigma}}_{kl}}{B} \tag{40}$$

Specific Formulation for Isotropic Cohesive Soils

The previous formulation for isotropic materials can be adjusted for isotropic cohesive soils by specifying a number of undetermined functions appropriate for the modelling of them within the critical state soil mechanics framework (Schofield and Wroth, 1968 and Wood, 1990). This can be done after some modifications or assumptions without altering any of the previous equations (Herrmann et al, 1987). As a first assumption, the associated flow rule is used which requires setting U instead of F in all the previous equations.

Hardening, Elastic Constants and Bounding Plastic Modulus Kp

The bounding plastic modulus $\bar{K}_p$ in terms of the state variables $\bar{I}$, $\bar{J}$, α and $I_0(e^p)$, on F = 0, has been defined as (Dafalias and Herrmann, 1980):

$$\bar{K}_p = \frac{1+e_{in}}{\lambda-\kappa}\left(\left\langle 1 - \frac{I_1}{I_0}\right\rangle + \frac{I_1}{I_0}\right)3F_{,\bar{I}}\,(F_{,\bar{I}}.\bar{I} + F_{,\bar{J}}.\bar{J}) \tag{41}$$

The tangent elastic bulk modulus is given as:

$$K = \frac{1+e_{in}}{3\kappa}\left(\langle I - I_1\rangle + I_1\right) \tag{42}$$

Bounding Surface

Fig. (1) shows a smooth surface consisting of two ellipses and one hyperbola with continuous tangents at the connecting points H and B. Using a composite surface, rather than a single one, yields a better description of the material response for heavily over-consolidated states (Al-Ebady, 2001).

The following specific forms are adopted:

For ellipse 1:

$$F = (\bar{I} - I_0)\left(\bar{I} + \frac{R-2}{R} I_0\right) + (R-1)^2\left(\frac{\bar{J}}{N}\right)^2 = 0 \qquad .(43)$$

For the hyperbola:

$$F = \left(\bar{I} - \frac{I_0}{R}\right)^2 - \left(\frac{\bar{J}}{N} - \frac{I_0}{R}\right)\left[\frac{\bar{J}}{N} - \frac{I_0}{R}\left(1 + 2\frac{RA}{N}\right)\right] = 0 \qquad (44)$$

For ellipse 2:

$$F = (\bar{I} - TI_0)\left[\bar{I} - (T + 2\zeta)I_0\right] + \rho\bar{J}^2 = 0 \qquad (45a)$$

$$\zeta = -\frac{T(Z + TF')}{Z + 2TF'} \; ; \rho = \frac{T^2}{Z(Z + 2TF')} \qquad (45b)$$

$$y = \frac{RA}{N}; \quad F' = \frac{N}{\sqrt{1+y^2}}; \quad Z = \frac{N}{R}(1 + y - \sqrt{1+y^2}) \qquad (45c)$$

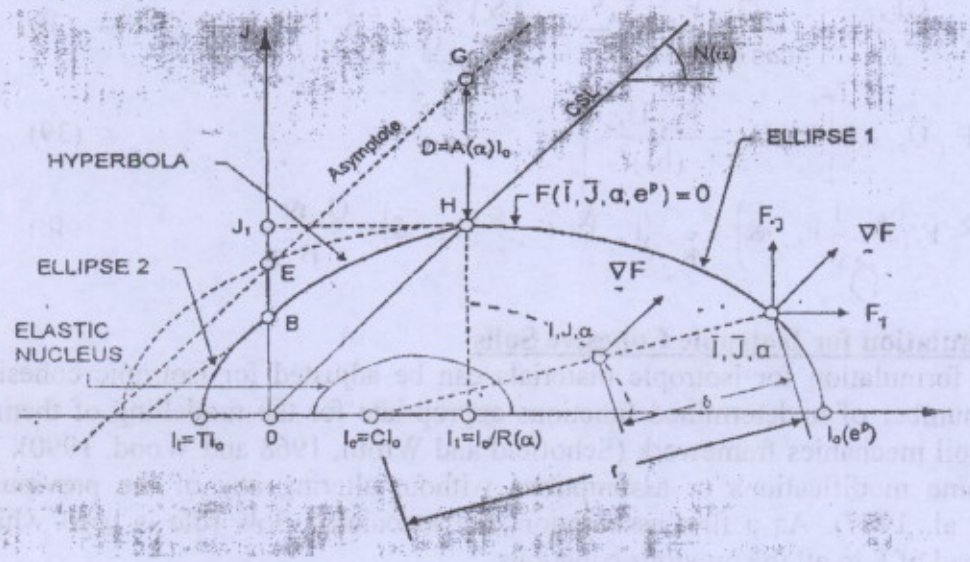

"Composite Form" of the Bounding Surface.

Fig. (1) A form of the radial mapping version of the bounding surface model in the invariant stress space (Dafalias and Herrmann,1986).

The Final Explicit Expressions of the Model

Equation (24) is written again for the sake of completeness:

$$\dot{\sigma}_{ij} = D_{ijkl}\,\dot{\varepsilon}_{kl} \qquad (46)$$

Combining Equations (32, 37-40, 41 and 42) with $R_{ij} = L_{ij}$ and $U_{ij} = F_{,ij}$ etc. expressions, representing the adoption of the associated flow rule: the explicit form of the D_{ijkl} tensor can now be determined as:

$$D_{ijkl} = G(\delta_{ki}\delta_{lj} + \delta_{kj}\delta_{li}) + \left(K - \frac{2}{3}G\right)\delta_{ij}\delta_{kl}$$

$$- \frac{\bar{h}(L)}{B}\left[3KF_{,i}\,\delta_{ij} + \frac{G}{J}F_{,j}\,s_{ij} + \frac{\sqrt{3}G}{\cos(3\alpha)}\frac{F_{,\alpha}}{bJ}\left(\frac{s_{in}s_{nj}}{J^2} - \frac{3S^3 s_{ij}}{2J^4} - \frac{2\delta_{ij}}{3}\right)\right]$$

$$\left[3KF_{,\bar{i}}\,\delta_{kl}+\frac{G}{J}F_{,\bar{j}}\,s_{kl}+\frac{\sqrt{3}G}{\cos(3\alpha)}\frac{F_{,\alpha}}{bJ}\left(\frac{s_{kn}s_{nl}}{J^2}-\frac{3S^3s_{kl}}{2J^4}-\frac{2\delta_{kl}}{3}\right)\right] \qquad (47)$$

in which

$$L=\frac{1}{B}\left\{3KF_{,\bar{i}}\,\dot{\varepsilon}_{kk}+\frac{G}{J}F_{,\bar{j}}\,s_{ij}\,\dot{\varepsilon}_{ij}+\frac{\sqrt{3}G}{\cos(3\alpha)}\frac{F_{,\alpha}}{bJ}\left[\left(\frac{s_{ik}s_{kj}}{J^2}-\frac{3S^3s_{ij}}{2J^4}\right)\dot{\varepsilon}_{ij}-\frac{2\dot{\varepsilon}_{kk}}{3}\right]\right\} \qquad (48)$$

$$B=K_p+9K(F_{,i})^2+G(F_{,j})^2+G\left(\frac{F_{,\alpha}}{bJ}\right)^2. \qquad (49)$$

where K is the elastic bulk modulus given by Equation (42) and G is the elastic shear modulus either defined independently or is computed from K and a specified value of Poisson's ratio. The plastic modulus K_p is obtained from Equation (31).

Equation (47) can now be used as the constitutive matrix representing isotropic cohesive soils in Equation (7c) for $\underline{\mathbf{D}}_T$ when substituted in Equation (17).

IDENTIFICATION OF THE INPUT MATERIAL PARAMETERS FOR AN IRAQI SOIL

The general version of the bounding surface model requires the determination of parameters which define the initial state of the material, as well as (depending on which version of the bounding surface is used) fifteen or seventeen separate model parameters associated with the elastoplastic response **Fig. (1).** The values of several of these parameters can be determined from standard soil mechanics parameters such as the compression index, the swell/ recompression index and the effective friction angle. Furthermore, the values of other parameters fall within fairly narrow ranges. Finally, the values, typically selected for many of these parameters are fixed for most soils; the total number of parameters, therefore, is substantially reduced. The reason for having a large number of parameters is the desire to account for even minute details of the stress-strain response. Simpler models that employ a lesser number of parameters cannot account for such details. If such perfection is not desired, the actual number of model parameters can be reduced to as low as six.

Testing Program

A comprehensive testing program, both in the field and laboratory, has been designed and executed to establish the required input soil parameters for soil samples extracted from a site in Baghdad, Iraq (Al-Busoda, 2004).

Field Tests

A continuous flight auger was used to obtain highly undisturbed soil samples, according to the procedures mentioned by Hvorslev (1949) and the US Corps of Engineers (1996). The samples were extracted from a site inside the campus at the University of Technology in Baghdad, Iraq (Figure 2) (Al-Busoda, 2004). Samples were taken from 3.5 to 7.5 meter depths.

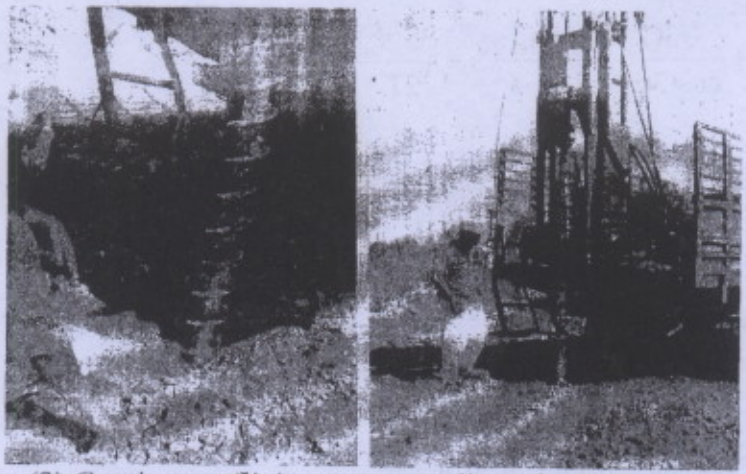

Fig. (2) Continuous flight auger sampling of a site in Baghdad
(from Al-Busoda, 2004)

Laboratory Tests

A series of classification, engineering and ultrasonic tests were performed in the laboratories at the Department of Civil Engineering of the University of Baghdad and the National Center for Engineering Laboratories and Research of the Ministry of Construction and Housing, Iraq.. The engineering tests included standard consolidation **Fig. (3),** cyclic consolidation **Fig. (4)** and triaxial tests. The stress conditions were according to the following:

- Isotropically consolidated undrained triaxial compression tests (ICUCT with OCR=1, 1.2 and 5) **Fig. (5).**
- Isotropically consolidated undrained triaxial extension tests (ICUET with OCR= 1, 1.2 and 5) **Fig. (6).**
- Ko consolidated undrained triaxial compression tests (KoCUCT with OCR = 1 and 2) **Fig. (7).**
- Ko consolidated undrained triaxial extension tests (KoCUET with OCR = 1) **Fig. (8).**

Accordingly, the soil was classified as an inorganic silty clay of high plasticity following the procedures adopted by the Unified Soil Classification System (USCS) (Al-Busoda [2004]). The soil will be termed henceforth as Baghdad brown silty clay.

After conducting calibration procedures, the input parameters for the bounding surface plasticity model for Baghdad brown silty clay obtained from field and laboratory tests are summarized in **Table (1)** along with the same properties for Boston blue clay.

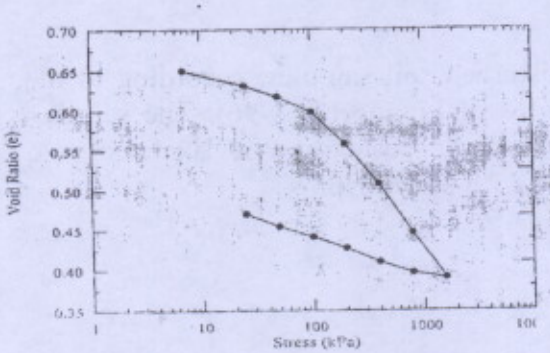

Fig. (3) Results of a standard consolidation test at depth (7-7.5m).

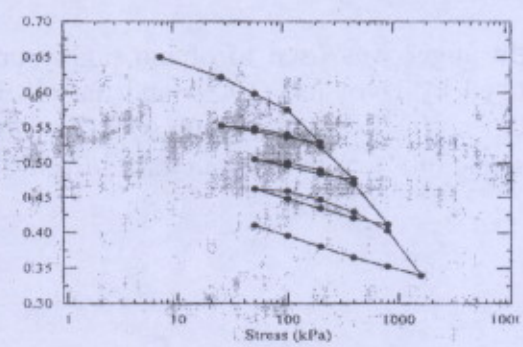

Fig. (4) Results of a cyclic consolidation test at depth (7-7.5m).

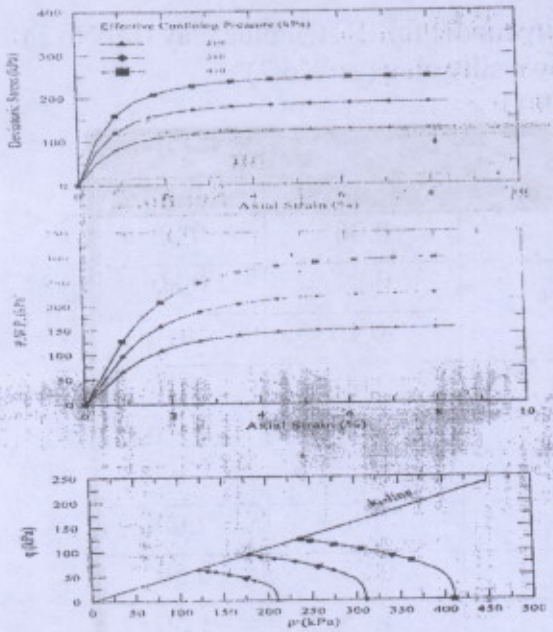

Fig. (5) Results of isotropically consolidated undrained triaxial compression tests at depth (7-7.5m).

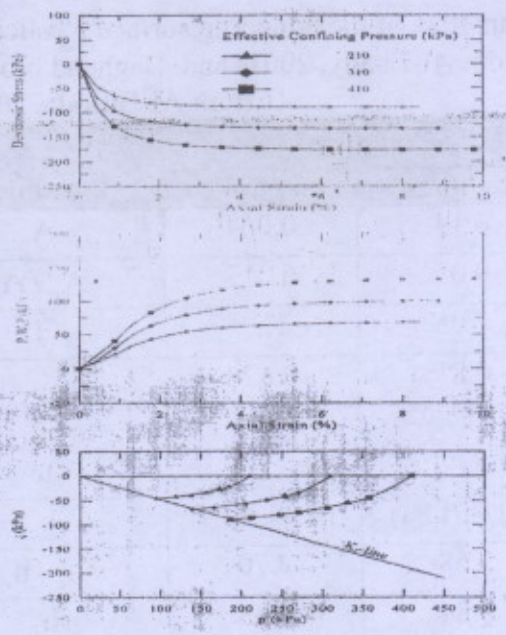

Fig. (6) Results of isotropically consolidated undrained triaxial extension tests at depth (7-7.5m).

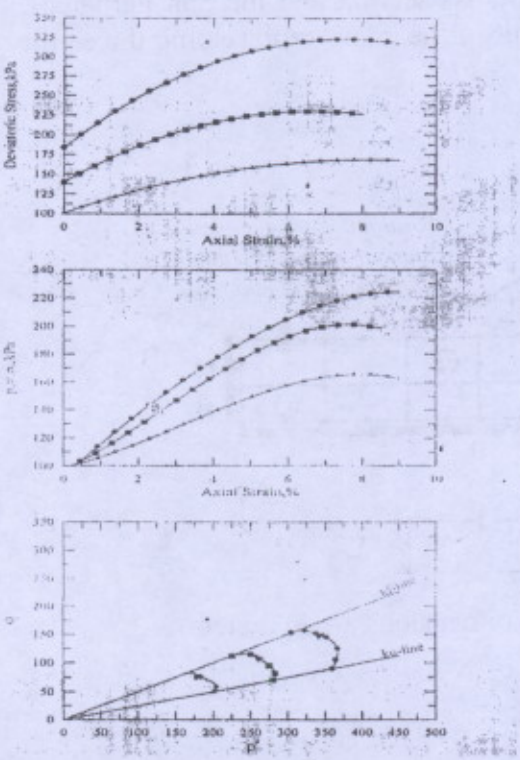

Fig. (7) Results of Ko consolidated undrained triaxial compression tests at depth (7-7.5m).

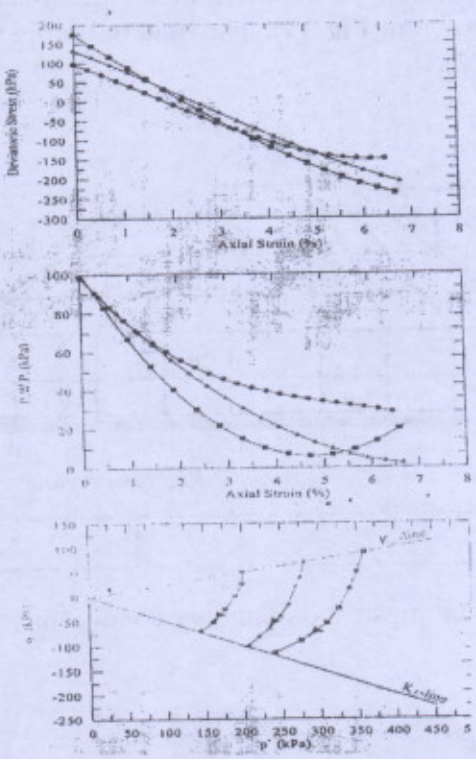

Fig. (8) Results of Ko consolidated undrained triaxial extension tests at depth (7-7.5m).

Table (1) Input parameters of the bounding surface plasticity model for Bosten blue clay (set No.1) (from Al-Ebady, 2001) and Baghdad brown silty clay (set No.2) (from Al-Busoda, 2004)

Parameter	Value		Parameter	Value	
	Set no. 1	Set no. 2		Set no. 1	Set no. 2
λ	0.14	0.064	A_c	0.06	0.05
κ	0.05	0.017	A_e / A_c	0.83	0.80
M_c	1.05	1.20	T	-0.10	-.010
M_e / M_c	0.81	0.676	C	0.00	0.00
υ	0.2	0.4	s	1.00	1.00
P_t	30.4 (kPa)	30.4 (kPa)	m	0.02	0.02
P_{atm}	101.4 (kPa)	101.4 (kPa)	h_c	2.0	2.00
R_c	2.68	2.70	h_e / h_c	0.75	0.50
R_e / R_c	0.84	0.85	h_0	1.75	1.50

NUMERICAL EXAMPLE: EARTH-DAM ANALYSES

The lower San Fernando earth-dam under the horizontal excitation of the San Fernando earthquake is analyzed. The real problem may be defined as a free fluid- pore fluid -solid interaction problem (i.e., a three field problem with class I plus class II couplings). The finite element mesh with detailed dimensions, material type numbers of the earth-dam cross section and the San Fernando earthquake record are shown in **Fig. (9).** The material properties of the zones representing the earth dam are listed in **Table (2).**

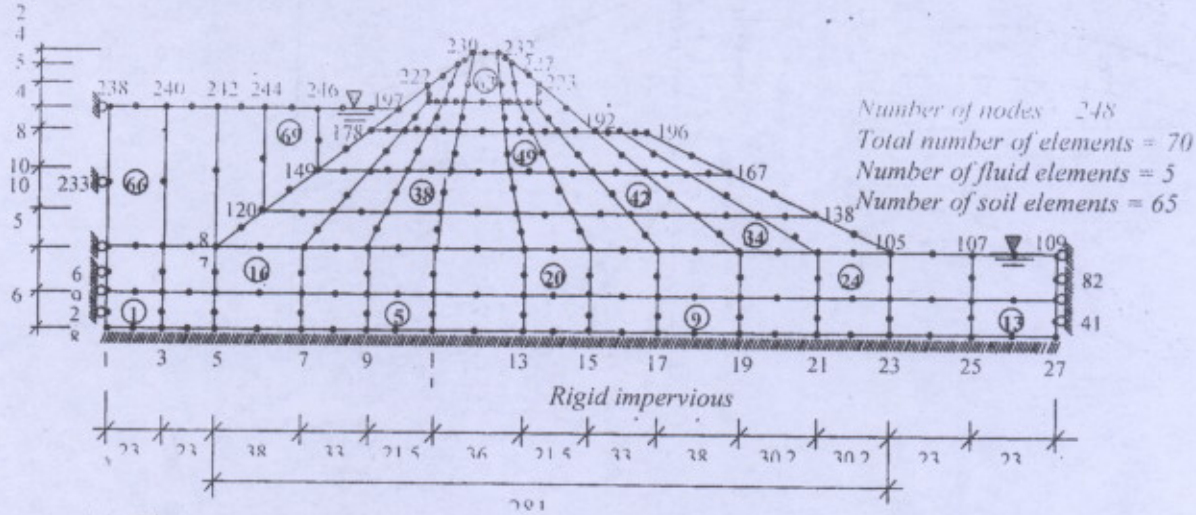

(a): Finite element mesh and boundary conditions (all dimensions are in meters).

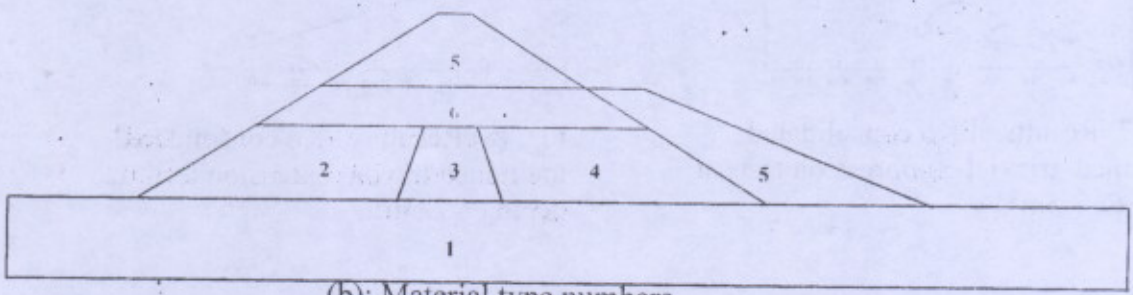

(b): Material type numbers.

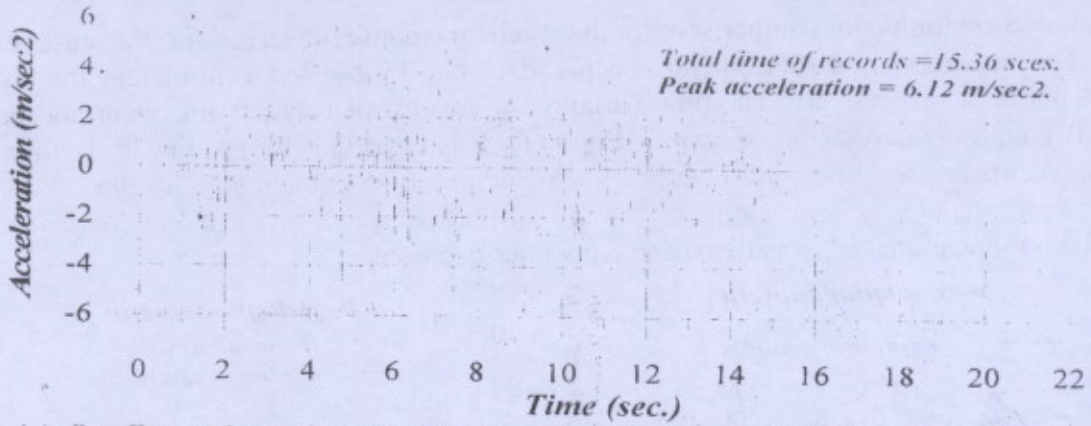

(c): San Fernando earthquake, N18E component, Feb. 9, 1971 (from Paul, 1982).

Fig. (9) Finite element mesh, material type numbers and San Fernando earthquake for an earth-dam problem (Zienkiewicz et al, 1984).

Table (2) Material properties of zones constituting earthen dam (Al-Tae'e, 2001).

	Material Zone	Dynamic elastic modulus (MN/m^2)	Dynamic Poisson's ratio υ	Strength parameters (MN/m^2)		Density (T/m^3)
				C	ϕ'	
1	Alluvium	200	0.40	10	38	2.090
2	Hydraulic fill sand	90	0.41	10	37	2.020
3	Clay core	90	0.41	10	37	1.800
4	Hydraulic fill sand	110	0.41	10	37	2.020-saturated 1.710-dry
5	Rolled fill	60	0.30	126	25	2.000
6	Ground shale hydraulic fill	90	0.41	10	37	2.020-saturated 1.710-dry

The analysis is performed in two stages: (1) Analysis of the earth-dam without pore pressure calculation within the soil and excluding the action of water in the reservoir (i.e., uncoupled solution). (2) Analysis of the earth-dam including the effect of water in the reservoir as finite elements and pore pressure calculation within the body of the dam (i.e., class I + II coupled solutions). The problem is solved by an implicit-implicit time marching scheme in which both the fluid and the soil are implicitly integrated in a staggered fashion at a time step length of $\Delta t = 0.001$ seconds. In these analyses, the clay core response is investigated by the use of the linear elastic model first with properties presented in **Table (2).** After that, the bounding surface plasticity model as described by section 4 of this paper using Boston blue clay and Baghdad brown silty clay properties presented in **Table (1)** is adopted for the clay core.

Fig. (10) shows the time-dependent variation of crest displacements (nodal point 232 in **Fig. (9a)**) for linear elastic and nonlinear bounding surface plasticity for Baghdad brown silty clay uncoupled analyses. It is noticed from **Fig. (10a)** that the x-displacement for both linear and nonlinear analyses oscillates around the zero-displacement axis and reaches a maximum value of 40 cm at 10 seconds with a slight difference in amplitudes. However, **Fig. (10b)** shows a significant difference in the amplitudes and phases of the y-displacements compared with that of the x- one **Fig. (10a)** for the elastic analysis. Also, the nonlinear analysis shows a subsequent drop of the amplitudes due to the

permanent deformations in comparison to the cyclic response observed in the case of linear analysis. The maximum y-displacements are found to be -35 and -55 centimeters for linear and nonlinear analyses, respectively. The time-variation of crest displacements for linear and nonlinear class I + II coupling analyses are shown in **Fig. (11).** It is clear that for the linear elastic analysis, the x- displacements decrease significantly at the beginning to -8 cm and then oscillate around -6 to -12 cm displacements values in comparison to 40 cm in the case of an elastic uncoupled solution. Also, in the nonlinear analysis, the displacement values decrease.

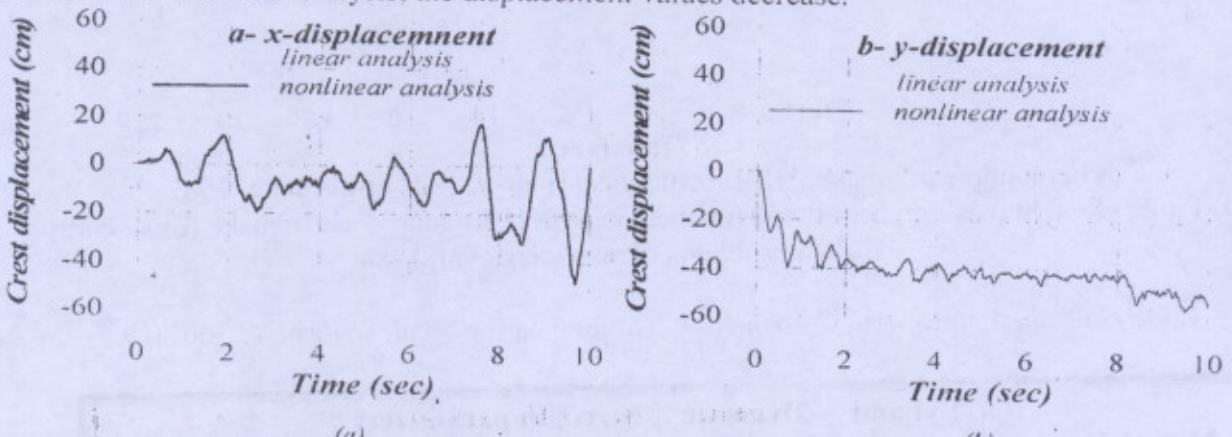

Fig (10) Variation of crest displacements with time for the uncoupled analysis.

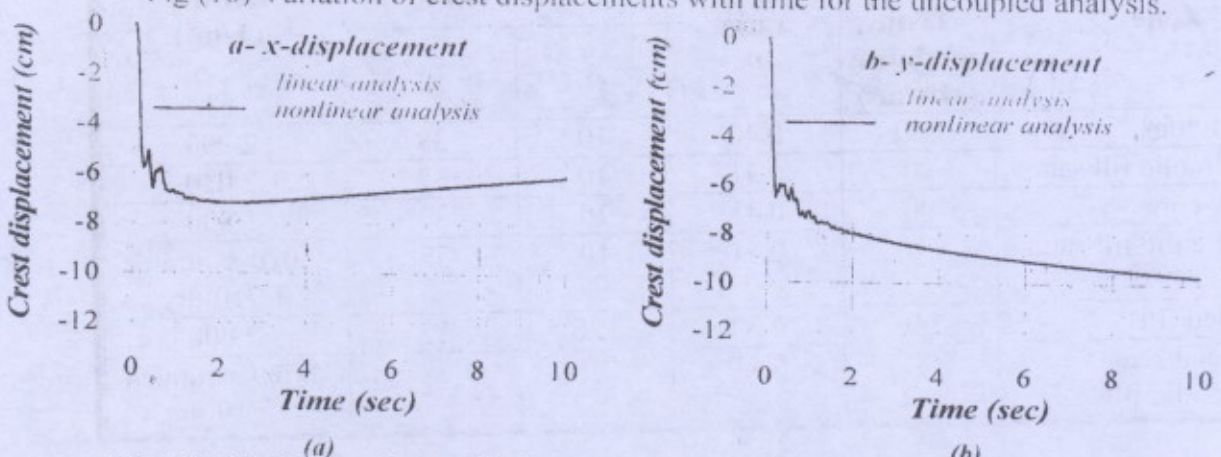

Fig. (11) Variation of crest displacements with time for class I + class II couplings.

The comparison between **Figs. (10) and (11)** shows that when including the action of water, the displacement response of the analyses is less than that without water being considered. Logically, this result is true due to the failure of the dam tending to occur towards the upstream side and the reaction of water represents a support that reduces the displacement response. Also, the water in the pores shares the solid in carrying the applied load. However, as time progresses, the excess pore water pressure which rises up and falls down under the applied loading becomes in a steadier state within the body of the dam.

Figs. (12), (13) and (14) show the contour lines of the vertical total and effective stresses and the excess pore water pressures for uncoupled and coupled analyses (at the end of 10 seconds). It is observed that the nonlinear soil response causes a pore pressure build-up which may lead to failure of the dam.

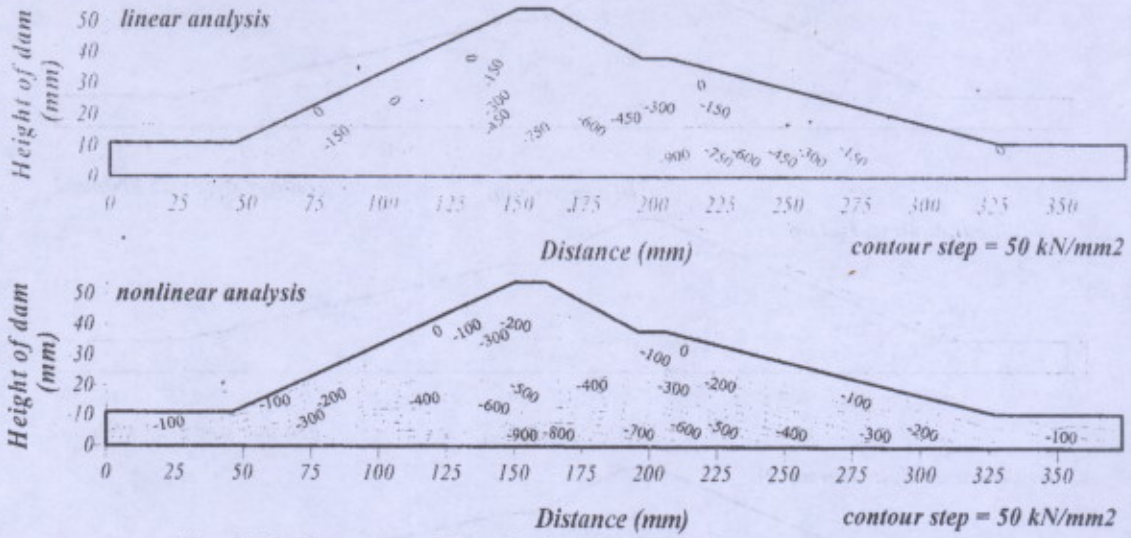

Fig. (12) Contours of vertical total stress for (uncoupled solution).

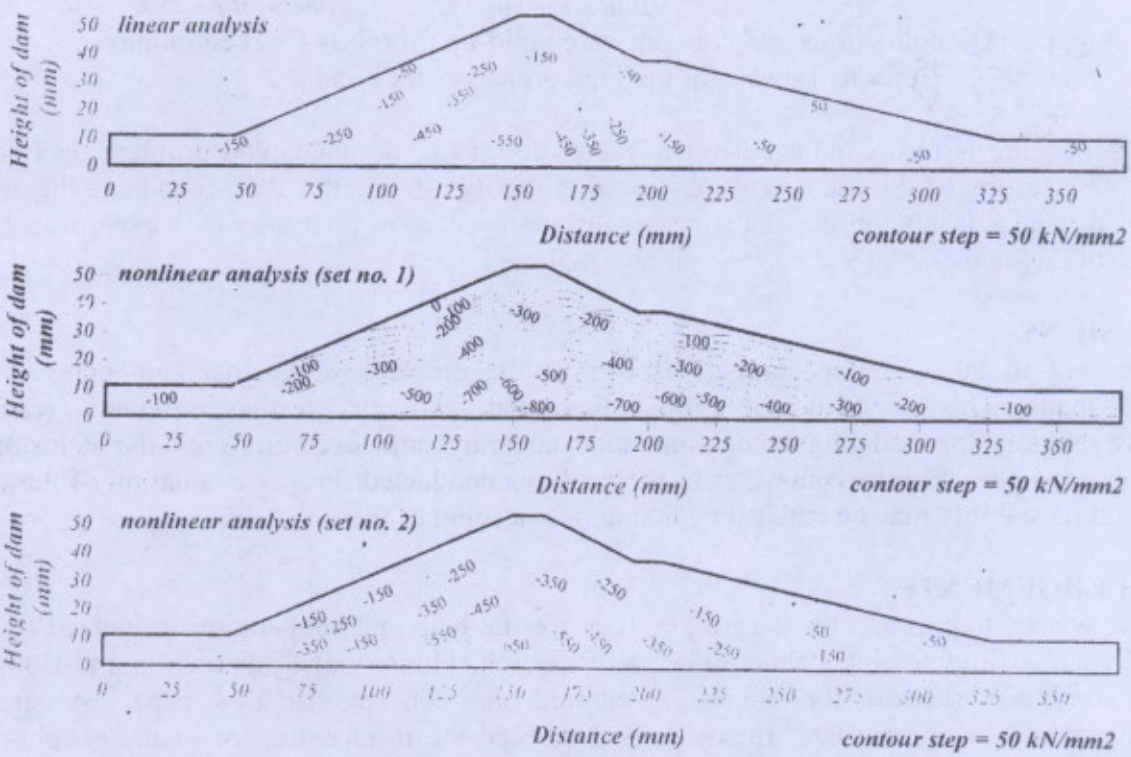

Fig. (13) Contours of vertical effective stress for (class I + II couplings) (refer to Table 1 for material property sets 1 and 2).

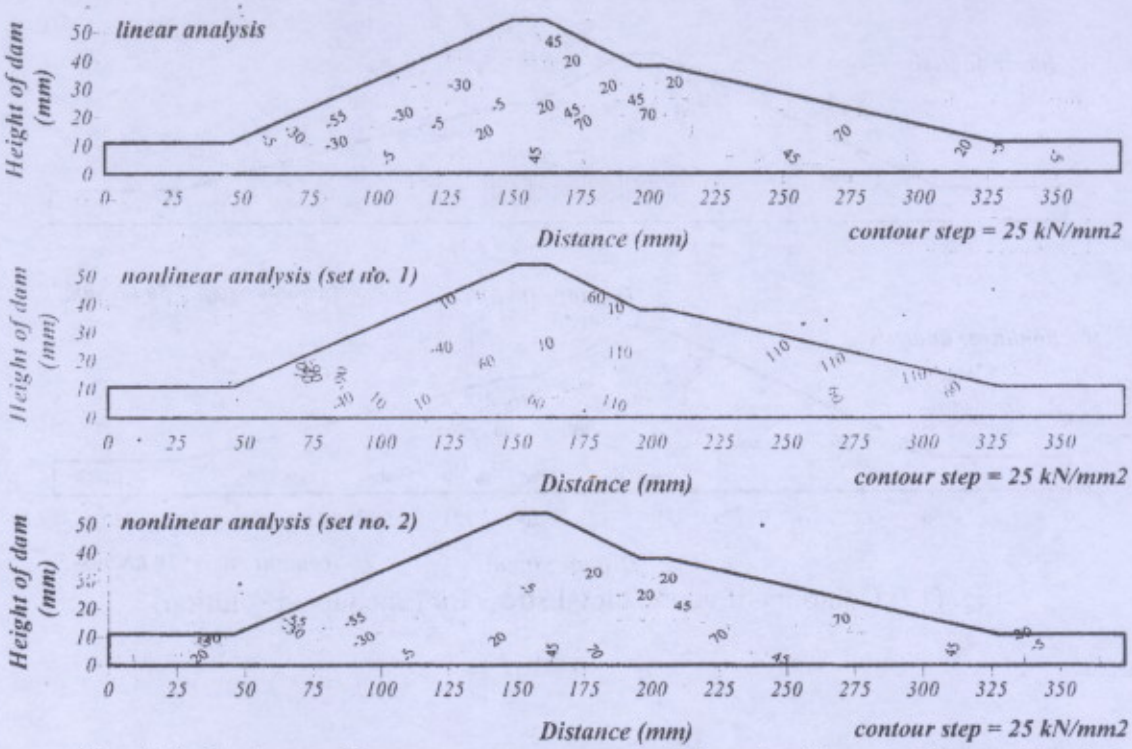

Fig. (14) Contours of excess pore pressure build-up for (class I + II couplings) (refer to Table 1 for material property sets 1 and 2).

A similar procedure is also conducted by Al-Tae'e (2001) for the uncoupled problem on Boston blue clay. The results of Al-Tae'e (2001) show that the dam fails after 2.5 seconds as the strain exceeds 5 % which is not observed in the results of the present analysis. This exemplifies the importance of the inclusion of water effects in the analyses.

CONCLUSIONS

It is important to take into account all aspects of the problem when analyzing dams under earthquake loads. This must include proper field and laboratory testing programs, realistic constitutive relations for modeling the dam materials under dynamic excitations and the inclusion of effects of pore water and reservoir water in the analyses conducted. Proper evaluation of the dam response and its stability may be reached by taking into account of these factors.

AKNOWLEDGEMENTS

The author wishes to express his sincere gratitude for the help and cooperation visualized by the National Center of Engineering Laboratories and Research, Ministry of Construction and Housing for their continued support throughout developing the concepts of this paper. A special acknowledgement goes to my late friend Mr Issam Saeed the former director of the geophysical laboratory there.

REFERENCES

Abbas, R.M., (2003), Non-Linear Dynamic Soil-Structure Interaction of Concrete Foundations Supported on Fully Saturated Clays, PhD thesis, College of Engineering, University of Baghdad.

Al-Ani, W. A. S., (2001), Dynamic Response of Underground Structures, M.Sc. Thesis, College of Engineering, University of Baghdad, Iraq.

Al-Busoda, B. S. Z., (2004), Static and Dynamic Non-Linear Soil Behaviour by the Bounding Surface Plasticity Model of an Iraqi Soil, Ph.D. Thesis, College of Engineering, University of Baghdad, Iraq.

Al-Damluji, O. F., (1994), Dynamic Penetration-Contact Problems with a Particular Reference to Porous Media, Ph.D. Thesis, College of Engineering, University of Baghdad, Iraq.

Al-Damluji, O. F. and Al-Ta'ee, A. Y., (2002), Earthquake Analysis of the Lower San Fernando Dam Using Elastic, Equivalent Linear and Bounding Surface Plasticity Models, Journal of Engineering, College of Engineering, University of Baghdad, Volume 9, No. 1, March.

Al-Damluji, O. F., Al-Sa'aty A. Y. T. and Al-Nu'aimi, R. M. S., (2005), Coupled Finite Element Analysis of a Dam Reservoir System Under Dynamic Loading, submitted to be published in al-Handassa Engineering Journal, College of Engineering, University of Baghdad.

Al-Ebady, A. N., (2001), Consolidation using Bounding Surface Plasticity Model, M.Sc. Thesis, College of Engineering, University of Baghdad, Iraq.

Al-Juboory, F. M. M., (2003), Seismic Analysis of Earth Dams Considereing Pore-Water Dynamic Interaction, Ph.D. Thesis, College of Engineering, University of Baghdad, Iraq.

Al-Nu'aimi, R.M.S., (2004), Non-Linear Analysis of Coupled Soil-Fluid-Structure Interaction Under Dynamic Loading, Ph.D. Thesis, College of Engineering, University of Baghdad,

Al-Sherefi, M. H., (2000), Non-Linear Dynamic Response of Soils, M.Sc. Thesis, College of Engineering, University of Baghdad, Iraq.

Al-Tae'e, A. Y., (2001), Dynamic Response of Embankments and Dams by the Finite Element Method, M.Sc. Thesis, College of Engineering, University of Baghdad, Iraq.

Dafalias, Y. F., (1975), On Cyclic and Anisotropic Plasticity: (i) A General Model Including Material Behaviour under Stress Reversals, (ii) Anisotropic Hardening for Initially Orthotropic Materials, Ph.D. Thesis, University of California, Berkeley.

Dafalias, Y. F., (1980), The Concept and Application of the Bounding Surface in Plasticity Theory, Physical Non-Linearities in Structural Analysis, IUTAM Symposium, Selies, France, May, Eds., Hult, J., and Lemaitre, J., Sprnger Verlag, Berlin, W. Germany, 1981, pp.56-63.

Dafalias, Y. F., (1986), Bounding Surface Plasticity. I: Mathematical Foundation and Hypoplasticity, Journal of Engineering Mechanics Division, ASCE, Volume 112, No. 9, September, pp. 966-987.

Dafalias, Y. F., and Herrmann, L. R., (1980), A Boundary Surface Soil Plasticity Model, International Symposium on Soils under Cyclic and Transient Loading, Swansea, UK, Volume 1.

Dafalias, Y. F., and Herrmann, L. R., (1982), Bounding Surface Formulation of Soil Plasticity, in Soil Mechanics-Transient and Cyclic Loads, Pande G. N., and Zienkiewicz, O. C., Eds., John Wiley and Sons, Chichester, U.K., pp.253-282.

Dafalias, Y. F., and Herrmann, L. R., (1986), Bounding Surface Plasticity. II: Application to Isotropic Cohesive Soils, Journal of Engineering Mechanics Division, ASCE, Volume 112, No. 12, December, pp. 1263-1291.

Desai, C. S., and Siriwardane, H. J. (1984), Constitutive Laws for Engineering Materials with Emphasis on Geologic Materials, Prentice-Hall, Inc., Englewood Cliffs, New Jersey.

Frank, M. W., (1994), Fluid Mechanics, Third Edition, McGraw-Hill, Inc., Chapters 8 and 9.

Herrmann, L. R., Kaliakan, V., Shen, C. K., Mish, K. D., and Zhu, Z., (1987), Numerical Implementation of Plasticity Model for Cohesive Soils, Journal of Engineering Mechanics Division, ASCE, Volume 113, No. 4, April, pp. 500-519.

Hvorslev, M.J., (1949), Subsurface Exploration and Sampling of Soils for Civil Engineering Purposes, Waterways Experiment Station.

Joseph, H. S., (1997), Fluid Mechanics, Springer, Chapters 2 and 3.

Kaliakin, V. N. and Dafalias, Y. F. (1990), Verification of the Elastoplastic Viscoplastic Bounding Surface Model for Cohesive Soils, Journal of Japanese Society of Soil Mechanics and Foundation Engineering, Volume 30, No. 3, September, pp. 25-3

Kaliakin, V. N. and Herrmann, L. R., (1987), Guidelines for Implementing the Elastoplastic-Viscoplastic Bounding Surface Model for Isotropic Cohesive Soils, Department of Civil Engineering Report, University of California, Davis, pp. 1-81.

Mroz, Z., and Zienkiewicz, O.C., (1984),Uniform Formulation of Constitutive Equations for Clays and Sands, Mechanics of Engineering Materials, C.S. Desai and R. H. Gallagher, Eds., John Wiley and Sons, Chichester, U.K., pp. 415-449.

Mroz, Z., Norris, V. A. and Zienkiewicz, O.C., (1978), An Anisotropic Hardening Model for Soils and its Application to Cyclic Loading, International Journal for Numerical and Analytical Methods in Geomechanics, Volume 2, pp. 203-221.

Mroz, Z., Norris, V. A. and Zienkiewicz, O.C., (1979), Application of an Anisotropic Hardening Model in the Analysis of Elastoplastic Deformation of Soils, Geotechnique, Volume 29, 1, pp. 1-34.

Naylor, D. J., and Pande, G. N., (1981), Finite Elements in Geomechanics, Pineridge Press Limited.

Paul, D. K., (1982),Efficient Dynamic Solutions for Single and Coupled Multiple Field Problems, Ph.D. Thesis, University College, Swansea.

Schofield, A., N., and Wroth, C. P., (1968), Critical State Soil Mechanics, McGraw-Hill, London, England.

US Corps of Engineers, (EM 110-1-1906), (1996), Soil Sampling,

Wood, D. M., (1990),Soil Behaviour and Critical State Soil Mechanics, Cambridge University Press.

Yang, B. L., Dafalias, Y. F., and Herrmann, L. R., (1985), A Bounding Surface Plasticity Model for Concrete, Journal of Engineering Mechanics Division, ASCE, Volume 111, No. EM3, March, pp.359-380.

Zienkiewicz, O. C., Wood, W. L., Hine, N. W. and Taylor, R. L. (1984), A Unified Set of Single Step Algorithms-Part I: General Formulation and Application, International Journal for Numerical Methods in Engineering, Volume 20, pp.529-552.

LIST OF SYMBOLS

B = Strain –displacement matrix.
c = Speed of sound.
$\underline{C}_s$ = Rayleigh damping matrix.
$\underline{C}_f$ =Compressibility matrix.
C_{ijkl} = Components of the elasticity tensor.
D_t = Constitutive matrix.
$\dot{\varepsilon}$ and $\dot{\varepsilon}$ = Elastic and plastic void ratios, respectively.
e and p superscripts= Denotes the elastic and plastic parts.
E_{ijkl} = Inverse of C_{ijkl} fourth order tensor.
G = Shear modulus.
$\bar{h}(L)$ = Heaviside step function defined as 1 for $L > 0$ and 0 at $L \leq 0$.
$\hat{H}$ = Positive shape hardening scalar function of σ_{ij} and q_n.
$\hat{i}$, $\hat{j}$, $\hat{k}$ = Unit vectors in x, y and z directions, respectively.
K = Bulk modulus .
$\underline{K}_s$ = Stiffness matrix.
$\underline{K}_f$ =Flow matrix.
K_p = Plastic modulus.
$\underline{L}$ = Coupling matrix .
L = Loading index.
L_{ij} = Loading direction.
$\underline{M}_s$ = Solid skelton mass matrix.
$\underline{M}_f$ =Fluid mass matrix.
$\underline{N}_p$ = Shape functions for pore pressure.
$\underline{N}_u$ = Shape functions for solid skeleton displacements.
P_f = Mass density.
P = Pressure above the hydrostatic value.
q_n = Plastic internal variables.
r_n = Direction of $\dot{\varepsilon}_n$.
R = Distance of α_{ij} from σ_{ij}.
R_{ij} = Direction of $\dot{\varepsilon}_{ij}^p$.
s = Elastic factor that determines indirectly the "elastic nucleus".
t = Surface traction.
T = Time.
$\dot{u}_x$, $\dot{u}_y$ and $\dot{u}_z$ = Velocity components in x, y and z directions, respectively.

α and β are Rayleigh damping constants.
ε_{ij} = Strains due to stresses and the superscripts.
Γ = Boundary surface.
κ = Swelling line slope.
λ = Normal consolidation line slope.

μ' = The dynamic viscosity of fluid.
σ_{ij} = Stress tensor.
Ω = The domain.
$\langle\ \rangle$ = Macauley brackets defining the operation $\langle L\rangle = \bar{h}(L)L$.
A superposed dot indicates the rate.